PERGAMON

International Journal of Solids and Structures 36 (1999) 4821–4840

INTERNATIONAL JOURNAL OF SOLIDS and STRUCTURES

Numerical calculation of the elastic and plastic behavior of saturated porous media

S. Breuer*, S. Jägering

Institute of Mechanics, FB 10, University of Essen, D-45117 Essen, Germany

Received 18 August 1997; accepted 30 May 1998

Abstract

In this investigation the field equations governing the mechanical behavior of a fluid-saturated porous media are analyzed and built up for the study of elastic dynamical problems and quasi-static problems in case of elastic–plastic material behavior. The investigations are limited to small deformation in order to apply a geometrical linear approach. The two constituents are assumed to be microscopically incompressible. A numerical solution is derived by means of the standard Galerkin procedure and the finite element method.

1. Introduction

Porous media are present in many fields of engineering science. For example soil consists of a portion of space occupied partly by a solid phase (solid skeleton) and partly by a void space filled with fluid. A further application of porous media are metal powders, which consist of grains as solid phase and gas in the void space. These metal powders are used in compaction processes in mechanical engineering. The mechanical behavior of a saturated porous medium is governed mainly by the interaction of the solid phase with the fluid phase. This interaction occurs in quasi-static problems, but is particularly strong in dynamic problems.

The equations governing the interaction of the solid and fluid media were first established for dynamic problems by Fillunger (1936). Another approach for dynamic problems was formulated by Biot (1955), who did not proceed from the basic equations of mechanics, but introduced quite a good model in an intuitive way. At a later stage Truesdell (1957) introduced, guided by the ideas of Stefan (1871), the mixture theory. Morland (1972) extended this theory and in time this concept (mixture theory, restricted by the volume friction concept, known in the literature as porous media theory) has been successfully developed by Bowen (1980), Mow et al. (1980), de Boer and Kowalski (1983), Ehlers (1989) and Bluhm (1997). A survey of the historical development of the porous

* Corresponding author

0020-7683/99/$ - see front matter
PII: S0020-7683(98)00267-4

media theory and a discussion of inconsistencies implicit in the mixture theory has recently been given by de Boer (1996). His work ends with an introduction of the model developed by de Boer (1996) and Bluhm (1997), which is the basis for the calculation shown in this paper.

Most of the problems of the two phase behavior of a fluid-saturated porous medium can only be predicted quantitatively by elaborate numerical computation, which fortunately today is possible due to the development of powerful computers. Only a few analytical solutions are available, which are used here to verify the numerical results based on the same theory. For practical work with arbitrary boundary conditions we must use the finite element method.

In this investigation we start with the basic equations of the porous media theory and build them up for the numerical calculation. In particular the solutions for a one- and two-dimensional consolidation problem and the wave propagation in a two phase porous media with incompressible constituents will be shown, as well as a compaction process of a metal powder.

In order to simplify the problem, thermal effects and exchanges of mass as well as moment of momentum supply between the constituents are excluded.

2. Governing equations

2.1. Concept of volume fractions and kinematics

The volume fractions n^α are defined as the local ratios of the constituent volume elements $\mathrm{d}v^\alpha$ with respect to the bulk volume element $\mathrm{d}v$ of the mixture ($\alpha = 1, \ldots, \kappa$, where κ is the number of constituents)

$$n^\alpha = \frac{\mathrm{d}v^\alpha}{\mathrm{d}v}. \tag{1}$$

As a consequence of (1), we can calculate the partial volumes of each constituent by weighting the bulk volume with the volume fractions

$$v^\alpha = \int_{B_S} n^\alpha \, \mathrm{d}v. \tag{2}$$

With the aid of this assumption we obtained from the following identities

$$v = \int_{B_S} \mathrm{d}v = \sum_{\alpha=1}^{\kappa} v^\alpha = \int_{B_S} \sum_{\alpha=1}^{\kappa} \mathrm{d}v^\alpha = \int_{B_S} \sum_{\alpha=1}^{\kappa} n^\alpha \, \mathrm{d}v, \tag{3}$$

the volume fraction condition

$$\sum_{\alpha=1}^{\kappa} n^\alpha = 1. \tag{4}$$

The volume fraction condition (4) plays an important role as a constraint in the constitutive theory of porous saturated media, see Nunziato and Passman (1981) or Bluhm and de Boer (1997).

Each of the constituents φ^α has a real density $\varrho^{\alpha R}$, which is defined as the mass of φ^α per unit of

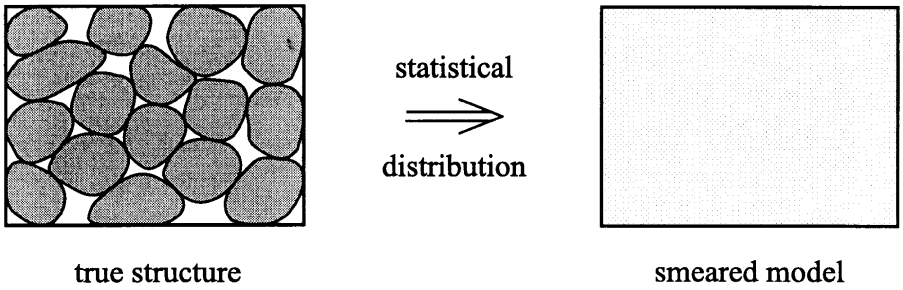

Fig. 1. Real structure and smeared model.

v^α. With the aid of the volume fraction concept these properties can be 'smeared' over the control space, see Fig. 1 and we have the partial density

$$\varrho^\alpha = n^\alpha \varrho^{\alpha R}. \tag{5}$$

In Fig. 1 the real structure of a porous medium is shown on the left side and the smeared model on the right side.

In the sequence the investigations are restricted to a binary model. Considering the kinematics of the fluid-saturated porous medium, which is an immiscible mixture of the constituents φ^α with particles X^α ($\alpha = S$: solid phase, $\alpha = F$: fluid phase), it is assumed that at any time t each spatial point $\mathbf{x}$ is simultaneously occupied by the particles X^S and X^F. These particles X^α proceed from different reference positions $\mathbf{X}_\alpha$ at time $t = t_0$. Thus, each constituent is assigned its own motion function $\boldsymbol{\chi}_\alpha$. The volumetric strain of each constituent, however, is restricted by the constraint (4). The velocity $\mathbf{x}'_S$ of the skeleton, its acceleration $\mathbf{x}''_S$ and deformation gradient $\mathbf{F}_S$ at an arbitrary point $\mathbf{X}_S \in B_0^S$ and an arbitrary instant of time t are described by

$$\mathbf{x} = \boldsymbol{\chi}_S(\mathbf{X}_S, t), \quad \mathbf{x}'_S = \mathbf{x}'_S(\mathbf{X}_S, t), \quad \mathbf{x}''_S = \mathbf{x}''_S(\mathbf{X}_S, t), \quad \mathbf{F}_S = \mathrm{Grad}_S\, \boldsymbol{\chi}_S, \tag{6}$$

where $\mathbf{x}$ denotes the current position of the point $\mathbf{X}_S$ and Grad_S means the derivative with respect to $\mathbf{X}_S$.

The motion of the fluid is given in the Eulerian way by the velocity field $\mathbf{x}'_F$ on the configuration space of point $\mathbf{x}$ and its acceleration $\mathbf{x}''_F$ is described by

$$\mathbf{x}'_F = \mathbf{x}'_F(\mathbf{x}, t), \quad \mathbf{x}''_F = \mathbf{x}''_F(\mathbf{x}, t). \tag{7}$$

Moreover, the Green strain tensor $\mathbf{E}_S$ is introduced

$$\mathbf{E}_S = \tfrac{1}{2}(\mathbf{F}_S^T \mathbf{F}_S - \mathbf{I}), \tag{8}$$

which can be expressed by the solid displacements $\mathbf{u}_S$. In the linearized form

$$\mathbf{E}_S = \tfrac{1}{2}(\mathrm{Grad}_S\, \mathbf{u}_S + \mathrm{Grad}_S^T\, \mathbf{u}_S) \tag{9}$$

is obtained.

2.2. Field equations

The mechanical behavior of a fluid-saturated porous solid is described in the porous media theory by the balance equation of mass for each individual constituent

$$(\varrho^{\alpha})'_{\alpha}+\varrho^{\alpha}\,\mathrm{div}\,\mathbf{x}'_{\alpha}=0, \tag{10}$$

the balance equation of momentum

$$\mathrm{div}\,\mathbf{T}^{\alpha}+\varrho^{\alpha}(\mathbf{b}-\mathbf{x}''_{\alpha})+\hat{\mathbf{p}}^{\alpha}=\mathbf{0} \tag{11}$$

and the volume fraction condition that changes for a binary mixture into the saturation condition

$$n^{S}+n^{F}=1. \tag{12}$$

In these equations $\mathbf{T}^{\alpha}$ is the partial Cauchy stress tensor, $\mathbf{b}$ the external acceleration and $\hat{\mathbf{p}}^{\alpha}$ the interaction force between the constituents. In addition, 'div' is the divergence operator and the symbol $(...)'_{\alpha}$ defines the material time derivative with respect to the trajectory of φ^{α}.

As the sum of the interaction forces must vanish, we obtain for a binary mixture

$$\hat{\mathbf{p}}^{F}+\hat{\mathbf{p}}^{S}=\mathbf{0}. \tag{13}$$

The balance equation of moment of momentum leads, excluding any moment of momentum supply, to symmetric stress tensors

$$\mathbf{T}^{\alpha}=\mathbf{T}^{\alpha T}. \tag{14}$$

Since both constituents are incompressible, we have:

$$\varrho^{\alpha R}=\text{constant}. \tag{15}$$

With this assumption, the volume fractions can be calculated from the balance equations of mass (10) and with the aid of the deformation gradient, one obtains

$$n^{\alpha}=n^{\alpha 0}(\det\mathbf{F}_{\alpha})^{-1}, \tag{16}$$

where $n^{\alpha 0}$ describes the initial porosity of φ^{α}.

2.3. Constitutive relations

In the above mentioned field equations the number of unknown variables is greater than the number of equations, thus, we have to close the problem with constitutive equations for the partial stress tensors $\mathbf{T}^{\alpha}$ and the interaction force $\hat{\mathbf{p}}^{F}$.

The constitutive relations for the solid and fluid stress tensors $\mathbf{T}^{\alpha}$ and for the interaction force $\hat{\mathbf{p}}^{F}$ consist of two terms,

$$\mathbf{T}^{\alpha}=-n^{\alpha}p\mathbf{I}+\mathbf{T}^{\alpha}_{E}, \tag{17}$$

$$\hat{\mathbf{p}}^{F}=p\,\mathrm{grad}\,n^{F}+\hat{\mathbf{p}}^{F}_{E}, \tag{18}$$

where the former, as a result of the saturation condition, is proportional to the pore pressure p, while the latter represents the extra quantities, index $(...)_{E}$, determined by the deformations.

In particular the viscosity of the fluid influences the interaction force $\hat{\mathbf{p}}^{\alpha}$, but with regard to the partial effective stress tensor of the fluid it can be neglected:

$$\mathbf{T}_E^F \approx \mathbf{0}. \tag{19}$$

In this investigation the applications are restricted to the geometrically linear theory, thus, the partial effective Cauchy stress tensor $\mathbf{T}_E^S$ of the solid and the second Piola Kirchhoff stress tensor $\mathbf{S}_E^S$ approximately coincide

$$\mathbf{T}_E^S \approx \mathbf{S}_E^S. \tag{20}$$

In the following the constitutive equations in the elastic, plastic and elastic–plastic states as well as the interaction supply will be developed.

(a) Elastic state

Within the framework of the geometrically linear theory $\mathbf{T}_E^S$ can be expressed by Hooke's law:

$$\mathbf{T}_E^S = \overset{4}{\mathbf{B}}_{Se}\mathbf{E}_{Se}, \tag{21}$$

for elastic material behavior $\mathbf{E}_{Se} = \mathbf{E}_S$ and for elastic–plastic behavior $\mathbf{E}_{Se}$ is the elastic part of the solid strain, as introduced in (32). The fourth-order tensor

$$\overset{4}{\mathbf{B}}_{Se} = 2\mu^S\overset{4}{\mathbf{I}} + \lambda^S\overset{4}{\bar{\mathbf{I}}} \tag{22}$$

is the constitutive tensor of elastic behavior. The response parameters λ^S, μ^S are the Lamé constants of the solid skeleton. The fourth-order tensors $\mathbf{I}$ and $\bar{\mathbf{I}}$ are identity tensors, as described in de Boer (1982).

(b) Plastic state

The plastic material behavior, as used in Section 5 of this paper, is governed by the yield function

$$F = II_{\mathbf{T}_E^{S^D}} + \tfrac{1}{2}\alpha^2 I_{\mathbf{T}_E^S}^2 - \tfrac{1}{2}\kappa^2 = 0, \tag{23}$$

see Green (1972) or de Boer and Kowalski (1983), where $II_{\mathbf{T}_E^{S^D}}$ is the second invariant of the deviatoric part of $\mathbf{T}_E^S$ and $I_{\mathbf{T}_E^S}$ is the first invariant of $\mathbf{T}_E^S$. The geometrical interpretation of the parameters α and κ can be read in Bluhm et al. (1996). The quantities α and κ are assumed to depend on the plastic work W_p. From (23) we obtain the condition of consistency

$$\mathrm{D}F = \frac{\partial F}{\partial \mathbf{T}_E^S}\cdot \mathrm{D}\mathbf{T}_E^S + \frac{\partial F}{\partial \alpha}\mathrm{D}\alpha + \frac{\partial F}{\partial \kappa}\mathrm{D}\kappa = 0, \tag{24}$$

where

$$\mathrm{D}\alpha = \frac{\partial \alpha}{\partial W_p}\mathrm{D}W_p = \frac{\partial \alpha}{\partial W_p}\mathbf{T}_E^S\cdot \mathrm{D}\mathbf{E}_{Sp} \tag{25}$$

and

$$\mathrm{D}\kappa = \frac{\partial \kappa}{\partial W_\phi}\mathrm{D}W_p = \frac{\partial \kappa}{\partial W_\phi}\mathbf{T}_E^S\cdot \mathrm{D}\mathbf{E}_{Sp}. \tag{26}$$

D represents the material time derivative with respect to the solid body. The loading criteria for hardening material can be derived from the consistency condition, see de Boer and Ehlers (1980), as

$$F=0 \quad \text{and} \quad \frac{\partial F}{\partial \mathbf{T}_E^S}\cdot \mathrm{D}\mathbf{T}_E^S \begin{cases} >0 \text{ loading} & \mathrm{D}\mathbf{E}_{Sp}\neq 0, \\ =0 \text{ neutral state} & \mathrm{D}\mathbf{E}_{Sp}=0, \\ <0 \text{ unloading} & \mathrm{D}\mathbf{E}_{Sp}=0 \end{cases} \tag{27}$$

and for ideal plastic material behavior as

$$F=0 \quad \text{and} \quad \frac{\partial F}{\partial \mathbf{T}_E^S}\cdot \mathrm{D}\mathbf{T}_E^S \begin{cases} =0 \text{ neutral state} & \mathrm{D}\mathbf{E}_{Sp}\neq 0, \\ <0 \text{ unloading} & \mathrm{D}\mathbf{E}_{Sp}=0. \end{cases} \tag{28}$$

In order to describe the complete motion of an initial- and boundary-value problem the associated flow rule

$$\mathrm{D}\mathbf{E}_{Sp}=\mathrm{D}\lambda\frac{\partial F}{\partial \mathbf{T}_E^S}, \tag{29}$$

with

$$\mathrm{D}\lambda=\frac{\dfrac{\partial F}{\partial \mathbf{T}_E^S}\cdot \overset{4}{\mathbf{B}}_{Se}\mathrm{D}\mathbf{E}_S}{\dfrac{\partial F}{\partial \mathbf{T}_E^S}\cdot \overset{4}{\mathbf{B}}_{Se}\dfrac{\partial F}{\partial \mathbf{T}_E^S}+h}, \tag{30}$$

where

$$h=-\left(\frac{\partial F}{\partial \alpha}\frac{\partial \alpha}{\partial W_p}+\frac{\partial F}{\partial \kappa}\frac{\partial \kappa}{\partial W_p}\right)\mathbf{T}_E^S\cdot\frac{\partial F}{\partial \mathbf{T}_E^S} \tag{31}$$

is used. For ideal plastic material behavior, as applied in Section 5, the hardening parameter h disappears. The rate $\mathrm{D}\mathbf{E}_{Sp}$ is the plastic component of the strain increment and $\mathrm{D}\lambda$ the plastic multiplier.

(c) Strain–stress relation for plastic material behavior

In order to develop the stress–strain relation for elastic–plastic deformations we commence from the additive decomposition of the rate of the total strain $\mathrm{D}\mathbf{E}_S$

$$\mathrm{D}\mathbf{E}_S=\mathrm{D}\mathbf{E}_{Se}+\mathrm{D}\mathbf{E}_{Sp}. \tag{32}$$

The elastic component of the strain increment can be described by Hooke's law (21) and (22)

$$\mathrm{D}\mathbf{E}_{Se}=\overset{4}{\mathbf{B}}_{Se}^{-1}\mathrm{D}\mathbf{T}_E^S. \tag{33}$$

Using well-known manipulations in plasticity, see de Boer and Ehlers (1980), we obtain

$$\mathrm{D}\mathbf{E}_S = \left(\overset{4}{\mathbf{B}}{}_{Se}^{-1} + \frac{1}{h} \frac{\partial F}{\partial \mathbf{T}_E^S} \otimes \frac{\partial F}{\partial \mathbf{T}_E^S} \right) \mathrm{D}\mathbf{T}_E^S. \tag{34}$$

As shown in de Boer and Ehlers (1980) the relation (34) can be inverted and one obtains:

$$\mathrm{D}\mathbf{T}_E^S = \overset{4}{\mathbf{B}}{}_{Sp} \mathrm{D}\mathbf{E}_S, \tag{35}$$

where

$$\overset{4}{\mathbf{B}}{}_{Sp} = \overset{4}{\mathbf{B}}{}_{Se} - \frac{\overset{4}{\mathbf{B}}{}_{Se} \frac{\partial F}{\partial \mathbf{T}_E^S} \otimes \overset{4}{\mathbf{B}}{}_{Se} \frac{\partial F}{\partial \mathbf{T}_E^S}}{h + \frac{\partial F}{\partial \mathbf{T}_E^S} \cdot \left(\overset{4}{\mathbf{B}}{}_{Se} \frac{\partial F}{\partial \mathbf{T}_E^S} \right)}. \tag{36}$$

The derivative is represented by

$$\frac{\partial F}{\partial \mathbf{T}_E^S} = = \mathbf{T}_E^{S^D} + \alpha^2 (\mathbf{T}_E^S \cdot \mathbf{I}) \mathbf{I}, \tag{37}$$

see de Boer and Kowalski (1983).

(d) Interaction

The interaction between the fluid and solid constituents, caused by the motions, can be described by the extra supply term of momentum

$$\hat{\mathbf{p}}_E^F = - \frac{(n^F)^2 \gamma^{FR}}{k^F} \mathbf{w}_F, \tag{38}$$

with $\mathbf{w}_F = (\mathbf{x}'_F - \mathbf{x}'_S)$ being the seepage velocity, γ^{FR} the real specific weight of the fluid and k^F the Darcy permeability parameter.

2.4. Modification of variables

As mentioned above the control space of our porous medium is shaped by the solid skeleton. Thus, not the absolute motion of the fluid is of interest, but the motion relative to the solid skeleton. Let us introduce in place of the absolute velocity $\mathbf{x}'_F$ of the fluid the seepage velocity $\mathbf{w}_F$, which is the fluid velocity relative to the motion of the solid, as mentioned above.

This quantity occurs in a natural way in the extra supply term of momentum, see (38). In the other equations the absolute velocity of the fluid has to be replaced by:

$$\mathbf{x}'_F = \mathbf{w}_F + \mathbf{x}'_S. \tag{39}$$

This modification has also an advantage in describing the boundary conditions. At a moving, undrained boundary it is easier to prescribe that no fluid comes out ($\mathbf{w}_F = 0$), than to prescribe that the velocity of the fluid is equal to the velocity of the skeleton ($\mathbf{x}'_F = \mathbf{x}'_S$). A disadvantage of this modification is to be seen when we want to substitute the acceleration of the fluid by the time

derivations of $\mathbf{w}_F$ and $\mathbf{x}'_S$. In this case we have to take the convective acceleration terms into account and we get:

$$\mathbf{x}''_F = (\mathbf{w}_F + \mathbf{x}'_S)'_S + \underbrace{\operatorname{grad}(\mathbf{w}_F + \mathbf{x}'_S)\mathbf{w}_F}_{\text{convective acceleration terms}}. \tag{40}$$

These convective acceleration terms in the fluid are in practice relatively insignificant in view of the shortcomings with which the permeability k^F is determined and analogous to Zienkiewicz and Shiomi (1984) these terms are to be omitted from here onwards.

2.5. Final equations

Summing up the assumptions of the previous sections and substituting the constitutive equation in the field equations we get a final set of three equations. At first, we take the balance equation of momentum for the solid phase, insert the assumption (17) for the stress tensor and (17) and (38) for the interaction force, thus obtaining:

$$\operatorname{div}(\mathbf{T}^S_E - n^S p\mathbf{I}) + \varrho^S\mathbf{b} - \varrho^S\mathbf{x}''_S - p\operatorname{grad} n^F + \frac{\gamma^{FR}(n^F)^2}{k^F}\mathbf{w}_F = \mathbf{0}. \tag{41}$$

This equation describes the forces acting on the solid phase. The stress tensor is split into an effective part, determined by the motion and the weighted pore pressure. The terms describing its own weight and acceleration are similar to the terms used in classical continuum mechanics of monophasic media, but this equation is extended by the interaction force. In the same manner we obtain an equation for the fluid phase, presented by:

$$\operatorname{div}(-n^F p\mathbf{I}) + \varrho^F\mathbf{b} - \varrho^F(\mathbf{w}'_F + \mathbf{x}''_S) + p\operatorname{grad} n^F - \frac{\gamma^{FR}(n^F)^2}{k^F}\mathbf{w}_F = \mathbf{0}. \tag{42}$$

Up to here we have two vectorial equations for the unknown motions of the solid and the fluid. Another unknown is the pressure p. Therefore, we take the mass balance equations, considering the incompressibility and the saturation condition. Doing this, we obtain:

$$\operatorname{div}(n^F\mathbf{w}_F + \mathbf{x}'_S) = 0, \tag{43}$$

which represents the volume balance equation of the whole mixture. As a result of the incompressibility, we can see that if one part of the volume is changing, for example $\operatorname{div}\mathbf{x}'_S$, the change of the divergence of the other part is constrained.

In order to solve the system of equations in an effective way and to match the problem to the boundary and initial conditions we have to appropriate the balance equations of momentum. Firstly, we combine the balance equations of momentum (11) of both the constituents

$$\operatorname{div}(\mathbf{T}^S_E - p\mathbf{I}) + (\varrho^S + \varrho^F)\mathbf{b} - \varrho^S\mathbf{x}''_S - \varrho^F(\mathbf{w}'_F + \mathbf{x}''_S) = \mathbf{0}, \tag{44}$$

thus, getting an equation that describes the balance equation of momentum of the whole mixture. The interaction terms vanish, the total stress tensor is the addition of the partial stress tensors and the external acceleration acts on both the constituents.

The balance equation of momentum of the fluid (42) and the volume balance eqn (43) close the set of equations, while substituting ϱ^{α} by (5).

The calculation of the mechanical behavior of a porous medium based on this theory is governed by these three equations. As unknowns the motion of solid, the motion of fluid and the pore pressure appear.

3. Numerical solution

The system of equations introduced in the previous section can be discretized by using the standard finite element procedures and weak forms of the appropriate equations. Details of such methods are well described by Zienkiewicz (1984) or Lewis and Schrefler (1987). A semi-discretization procedure is used by approximating the unknown functions in the space domain. The time integration will be done by the standard Newmark method, by choosing the parameters $\beta = 0.25$ and $\delta = 0.5$.

3.1. Weak formulation

For numerical computations, a standard Galerkin procedure is chosen. Therefore, each of the basic equations (42)–(44) must be multiplied by a weighting function. These weighting functions have to satisfy the natural boundary conditions. For eqn (44) a virtual solid displacement $\bar{\mathbf{u}}_S$ is applied. The volume integral of a divergence can be transformed into a surface integral (Gauss theorem), see de Boer (1982), in order to prescribe static boundary conditions:

$$\int_B [(\mathbf{T}_E^S - p\mathbf{I}) \cdot \operatorname{grad} \bar{\mathbf{u}}_S + \varrho^S \mathbf{x}_S'' \cdot \bar{\mathbf{u}}_S + \varrho^F (\mathbf{w}_F + \mathbf{x}_S')_S' \cdot \bar{\mathbf{u}}_S] \, \mathrm{d}v = \int_A \mathbf{t} \cdot \bar{\mathbf{u}}_S \, \mathrm{d}a + \int_B (\varrho^S + \varrho^F) \mathbf{b} \cdot \bar{\mathbf{u}}_S \, \mathrm{d}v, \quad (45)$$

where $\mathbf{t}$ is the total stress vector at the surface of the mixture, consisting of the stress at the solid and the stress at the fluid.

Equation (42) is weighted by a virtual seepage velocity $\bar{\mathbf{w}}_F$ and the volume integral was transformed into a surface integral

$$\int_B \left\{ (-p \operatorname{div} \bar{\mathbf{w}}_F) + \frac{\gamma^{FR} n^F}{k^F} \mathbf{w}_F \cdot \bar{\mathbf{w}}_F + \varrho^{FR} (\mathbf{w}_F + \mathbf{x}_S')_S' \cdot \bar{\mathbf{w}}_F \right\} \mathrm{d}v = -\int_A p \bar{\mathbf{w}}_F \cdot \mathbf{n} \, \mathrm{d}a + \int_B \varrho^{FR} \mathbf{b} \cdot \bar{\mathbf{w}}_F \, \mathrm{d}v. \quad (46)$$

Equation (43) closes the set of equations. It represents the volume balance equation of the whole mixture and was multiplied by a virtual pressure $\bar{p}$:

$$\int_B \operatorname{div} (n^F \mathbf{w}_F + \mathbf{x}_S') \bar{p} \, \mathrm{d}v = 0. \quad (47)$$

Equation (47) causes numerical problems in this form. In two-dimensional problems with asymetric boundary conditions the pore pressure oscillates with large amplitudes with increasing depth. In

order to avoid this problem we follow a strategy suggested by Diebels and Ehlers (1995). Therefore, we take the balance equation of momentum of the fluid (42) and solve this equation explicitly for $\mathbf{w}_F$. Next we replace $\mathbf{w}_F$ in eqn (47) by this expression and after some transformations and changes we obtain:

$$\int_B \operatorname{div}\left[-\frac{k^F \varrho^{FR}}{\gamma^{FR}}(\mathbf{w}'_F+\mathbf{x}''_S)+\mathbf{x}'_S\right]\bar{p}\,\mathrm{d}v-\int_B \frac{k^F \varrho^{FR}}{\gamma^{FR}}\left[\mathbf{b}-\frac{1}{\varrho^{FR}}\operatorname{grad} p\right]\cdot\operatorname{grad}\bar{p}\,\mathrm{d}v$$
$$=-\int_A\left[\frac{k^F \varrho^{FR}}{\gamma^{FR}}(\mathbf{w}'_F+\mathbf{x}''_S)+n^F\mathbf{w}_F\right]\cdot\mathbf{n}\bar{p}\,\mathrm{d}a. \tag{48}$$

With this combination of eqns (42) and (43) the numerical problems vanish and the oscillation of the pore pressure fades away.

4. Examples for elastic material behavior

4.1. Verification of the chosen solution algorithm

Taking linear elasticity theory into account, de Boer et al. (1993) presented an analytical solution for a one-dimensional consolidation problem using the Laplace transformation.

Thus, there is an excellent example for the comparison of the analytical and the numerical solution. This test was introduced by Ehlers and Diebels (1994) in order to verify their chosen solution strategy. In this investigation the test has been repeated for the verification of the applied solution strategy, which differs in element shape, time integration and chosen shape functions from the above mentioned approach.

In order to model the half space via the finite element method, a column of 10 m depth and 2 m^2 surface was taken into account. The solution was only calculated for a very short time, so that no signal of the rigid boundary at a depth of 10 m could influence the solution.

The upper boundary of the column is perfectly drained and loaded once by a sine load (q):

$$q_1(t) = 3(1-\sin(\omega t))[\mathrm{kN/m^2}], \quad \omega = 75\ \mathrm{s}^{-1}, \tag{49}$$

and in another case by a step load (q):

$$q_2(t) = 3[\mathrm{kN/m^2}]. \tag{50}$$

The other boundaries are undrained and rigid, see Fig. 2. The material parameters are taken from de Boer et al. (1993) as:

$$\mu^S = 5583\ \mathrm{kN/m^2}, \quad \lambda^S = 8375\ \mathrm{kN/m^2},$$
$$\varrho^{SR} = 200\ \mathrm{kg/m^3}, \quad \varrho^{FR} = 1000\ \mathrm{kg/m^3},$$
$$n^S_{0S} = 0.67, \quad k^F = 0.01\ \mathrm{m/s}.$$

Figure 3 shows the surface displacement under both loads. It shows a good agreement between the analytical and the numerical solution. In the case of the step load the displacement–time

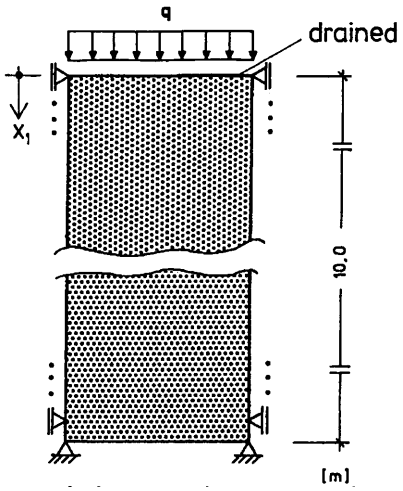

Fig. 2. Geometry of the one-dimensional consolidation problem.

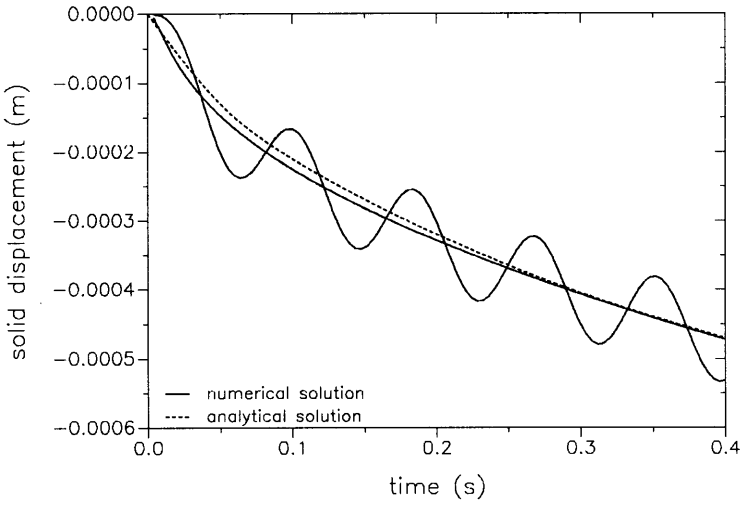

Fig. 3. Comparison between an analytical and a numerical solution.

behavior starts with a big time gradient, which decreases with increasing time, see Fig. 3. This is the typical behavior of an overdamped vibration-system, which has in fact the same structure after the discretization.

Considering the sine load the displacement–time behavior starts with a smoother time gradient and we obtain an exact agreement with the analytical solution.

4.2. Consolidation problem

As a next example the two-dimensional consolidation problem is going to be calculated. This class of problem occurs in soil mechanics, when foundations of buildings are the point of interest,

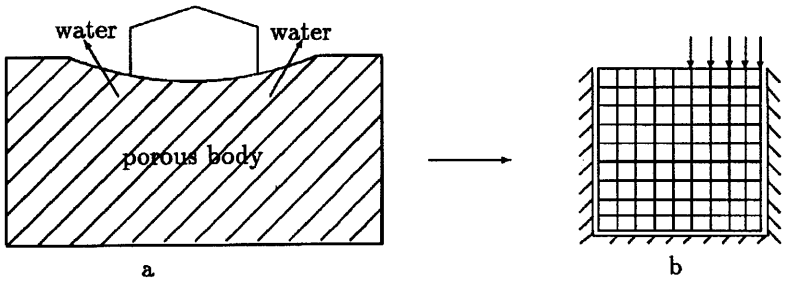

Fig. 4. Consolidation problem.

see Fig. 4a. Many computations are done in this field, for example Prévost (1981), Zienkiewicz and Shiomi (1984), Lewis and Schrefler (1987) or Ehlers and Diebels (1995). If we take the simplest case into account, the boundary conditions are symmetric and we have only to model one half of the problem (Fig. 4b). Therefore, an area of 10×10 m is taken into account. The material parameters are the same as in the previous section, except the Darcy-parameter. This parameter is changed to $k^F = 10^{-9}$ m/s in order to force a stronger coupling between the constituents.

In order to create an FE-model for the above mentioned problem, we discretize the plane of 10×10 m by 361 four-node rectangular elements and prevent the vertical solid displacements and the fluid motion at the bottom, as well as the horizontal solid displacements and fluid motion on both sides. At the top the left side is unloaded and drained, whereas the right side is undrained and loaded by a force, which simulates the weight of a building.

The consolidation process takes five years until the settlement reaches its final value, while the pore pressure decreases to zero. Figure 5 shows the pore pressure at different time steps.

In Fig. 5 we can see that in the beginning ($t = 1$ day) the whole external load (15 kN/m^2) is carried by the water and the pore pressure under the external load is as high as 14 kN/m^2. With the passage of time, the pore pressure decreases and after three years it is nearly zero.

Figure 6 shows the evolution of the solid displacement as a function of time. In the beginning only a small amount of drainage occurs. The ground on the right side moves down and as a result of the incompressibility, the ground on the left side moves up in the same way. With the passage of time the right side is still moving down whereas the left side stops moving up and starts with its settlement. During this time the water squeezes out of the porous body and after five years the process is finished, the settlement reaches its final value and the pore pressure is zero.

Figure 7 shows a vector plot of the seepage velocity at $t = 1$ day. The directions of the seepage velocity do not vary. The values of the velocity starts with large quantities and tend to zero after five years.

4.3. Wave propagation

In this section the wave propagation in a porous media is taken into account. According to Biot's theory, see Biot (1956) with two compressible constituents there are two longitudinal waves in a porous medium. One wave of dilatation is transmitted through the compressibility of the fluid and solid, the other is transmitted through the elastic structure.

These two waves are coupled through the stiffness of the soil and fluid components of the system

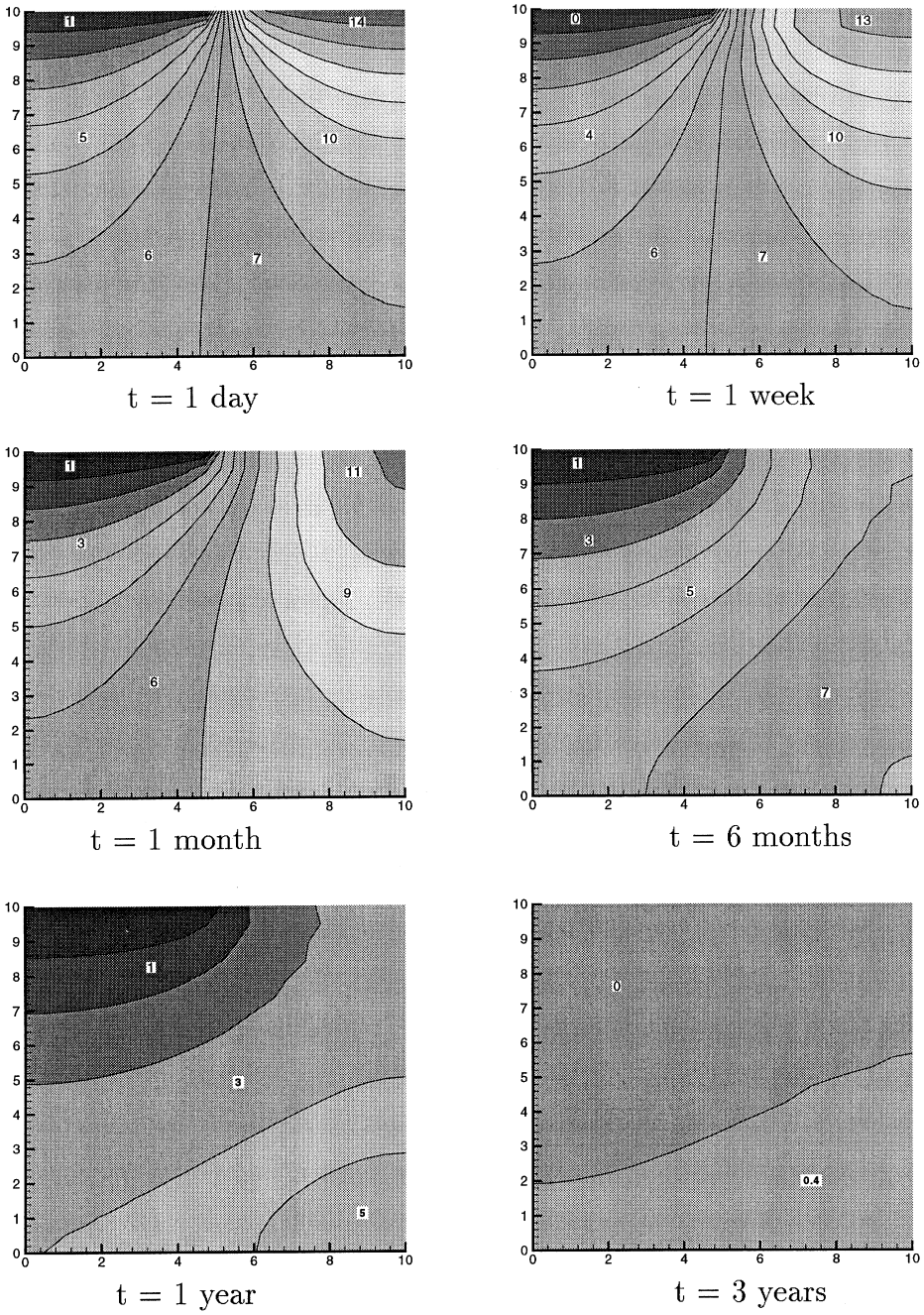

Fig. 5. Evolution of the pore pressure [kN/m^2] as a function of time.

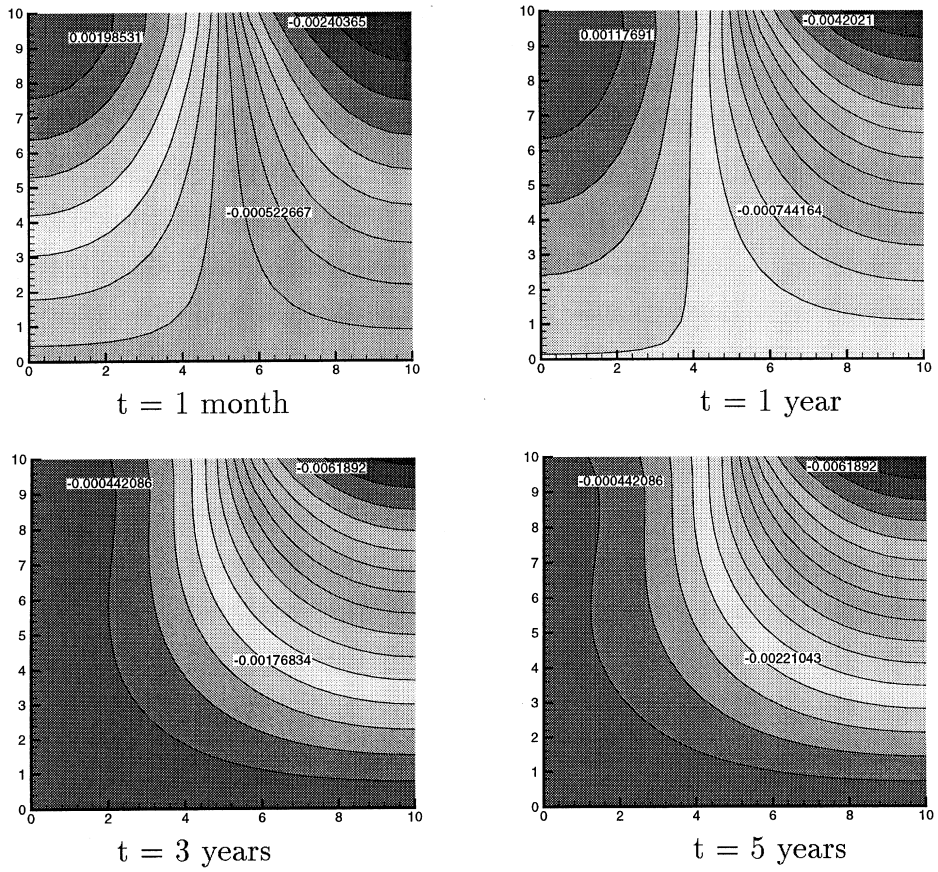

Fig. 6. Evolution of the solid displacement [m] as a function of time.

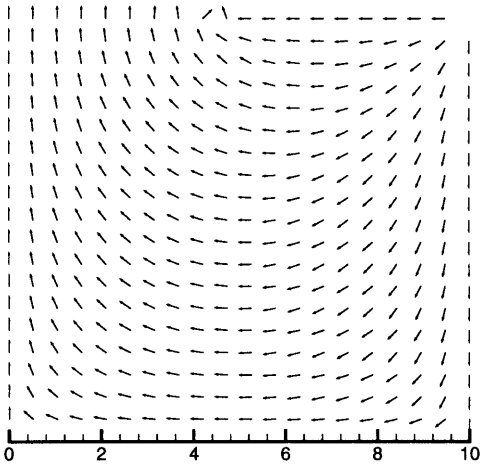

Fig. 7. Vector plot of the fluid motion at $t = 1$ day.

as well as through the coupling effect produced by motions of the solid and fluid, see Richart et al. (1970).

In this investigation both constituents are incompressible, thus the speed of the fast longitudinal wave is infinite. The wave motion which we can observe is the motion transmitted through the elastic structure of the solid skeleton.

The wave propagation in a one-dimensional porous body has been the topic of a former investigation, see Breuer (1997). In this paper the propagation of longitudinal and transverse waves in a two-dimensional body are the point of interest. Therefore, we take the same structure as in the previous section, but modeled with a hole in the middle of the plane. A sinusodal impulse pressure:

$$p(t) = \begin{cases} 100 \sin(78.54 \cdot t)[\mathrm{kN}] & \text{if } t \leqslant 0.04 \text{ s} \\ 0 & \text{if } t \geqslant 0.04 \text{ s} \end{cases}, \tag{51}$$

is applied at the surface of the hole in the center of the structure. The top is drained and unloaded.

Figure 8 shows the amount of the solid displacements u,

$$u = \sqrt{\mathbf{u}_1^2 + \mathbf{u}_3^2}, \tag{52}$$

at different time steps. The disturbance propagates in all directions with the same velocity. As expected, this causes a circle-form of the spread of the disturbance. Since the top is not a rigid boundary, the structure is smoother in this area and the displacements are larger. With passing time ($t = 0.04$ s) a reflection of the disturbance at the rigid and free boundary can be observed. The velocity of the longitudinal wave is exactly the same as calculated in the one-dimensional problems.

5. Examples for plastic material behavior

In the following section the compaction of a T-shaped die under plane strain is taken into account to show an example for the plastic material behavior. Since the investigations taken under consideration are slow processes, the inertia forces are neglected. A quasi-static solution has been computed. According to an example given in the literature by Morimoto et al. (1982), the die consists of a metal powder. This powder is modelled by the theory of porous media (TPM) as a powder skeleton with gas filled pores. The elastic material parameters of the powder are taken from the above mentioned literature as

$$E^S = 12{,}000 \text{ kN/m}^2, \quad \nu^S = 0.08.$$

The plastic material parameter for the Green yield function, see Section 2, are determined as

$$\alpha = 0.2, \quad \kappa = 0.6.$$

The properties of the gas are assumed to be negligible. The wall friction is assumed to depend on the normal stress at the wall and is calculated by using Coulomb's friction law. The results based on the theory of porous media are compared to the numerical and experimental results given in Morimoto et al. (1982).

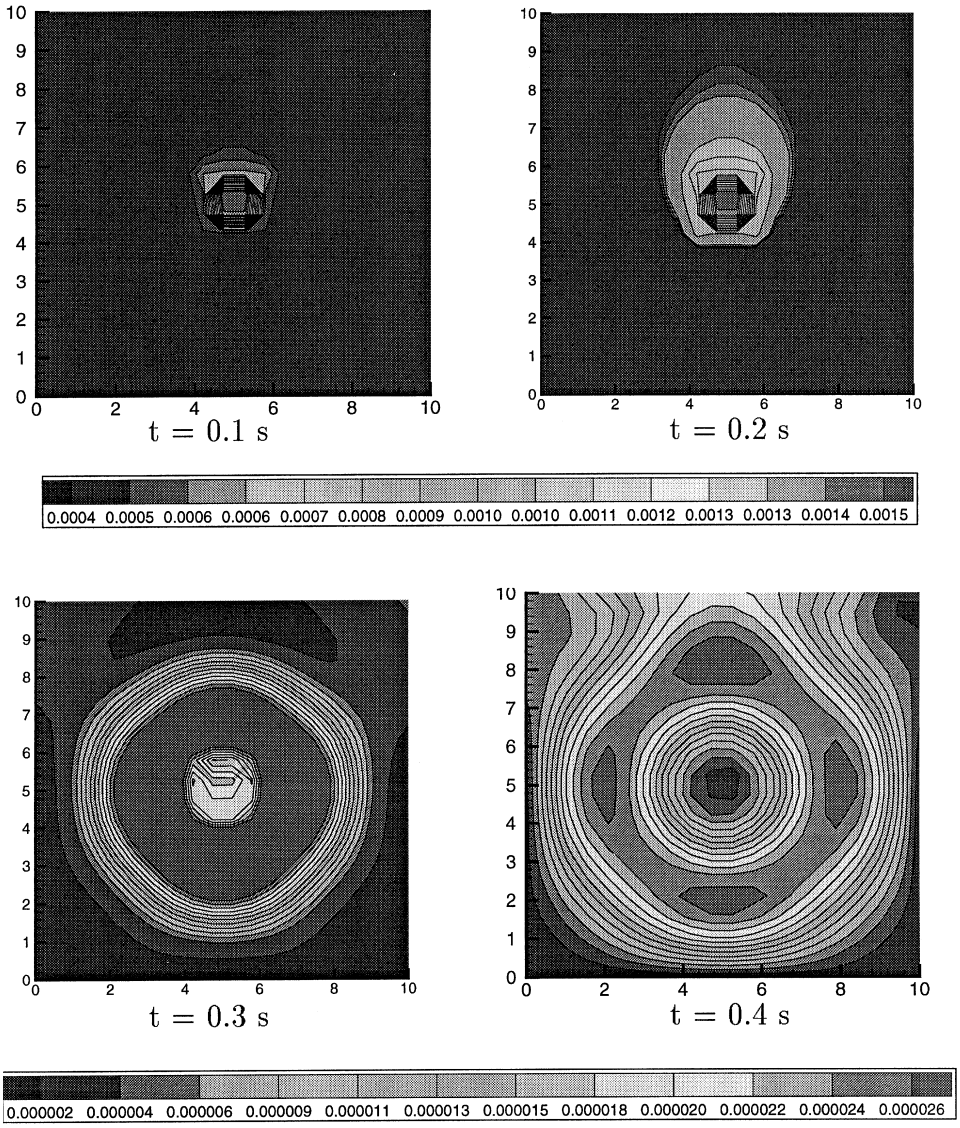

Fig. 8. Solid displacements [m].

Two different transformation processes are considered, first the displacements of the upper punch are prescribed and in a second case the punch movement of the bottom is prescribed. For the basic die design see Morimoto et al. (1982). Figures 9 and 10 show the relative density of the powder at the end of the process. The relative density

$$\varrho^{\mathrm{rel}} = \frac{\varrho^{S}}{\varrho^{SR}} = n^{S} \tag{53}$$

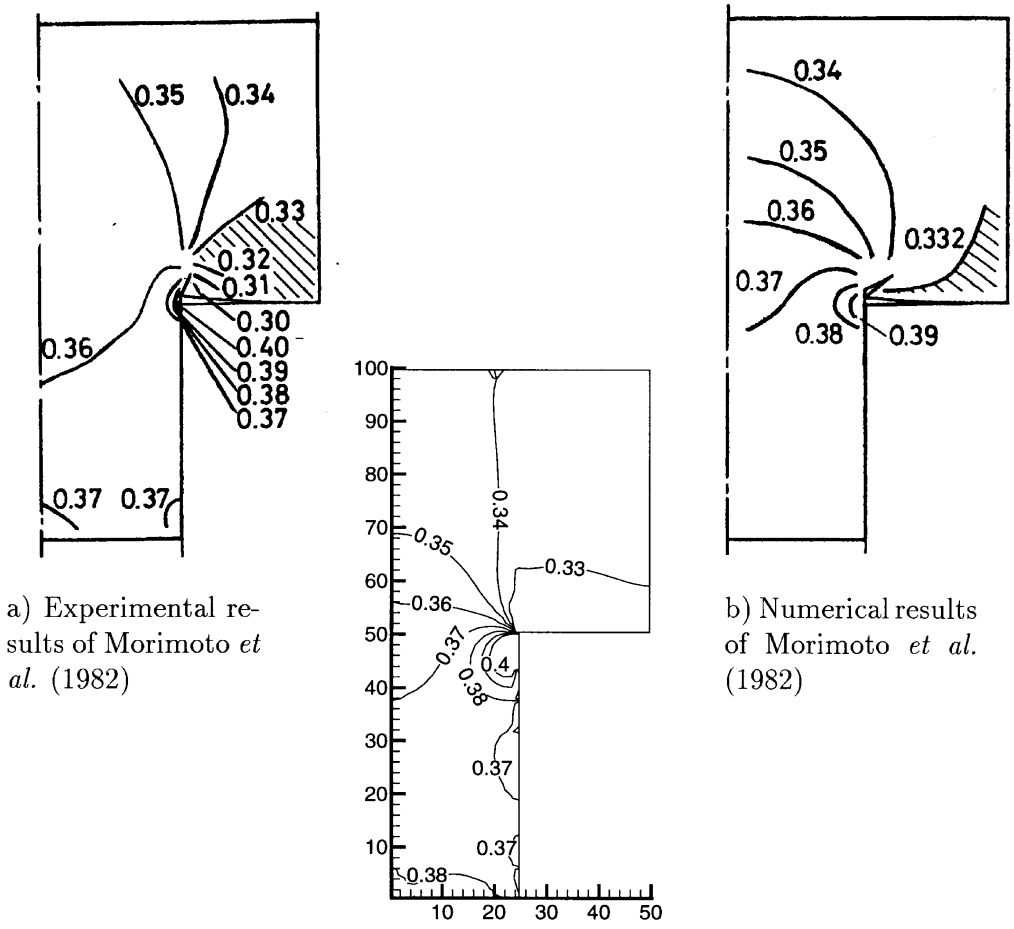

a) Experimental results of Morimoto *et al.* (1982)

b) Numerical results of Morimoto *et al.* (1982)

c) Numerical results based on the TPM

Fig. 9. Relative density (volume fraction of the solid) of the first case. (a) Experimental results of Morimoto et al. (1982). (b) Numerical results of Morimoto et al. (1982). (c) Numerical results based on the TPM.

is defined as the ratio of the apparent density to the maximum theoretical density. In the theory of porous media this quantity means the volume fraction of the solid.

The structure is modelled by 480 rectangular four-node elements and as the solution strategy the Newton–Raphson interaction, see Bathe (1990) was chosen.

5.1. Die compaction—movement of the lower punch

In the first case the lower punch moves up with a velocity of 0.5 mm/min until it reaches its final displacement of 8 mm. The punch at the top is fixed. The initial density is 0.332. The friction factor

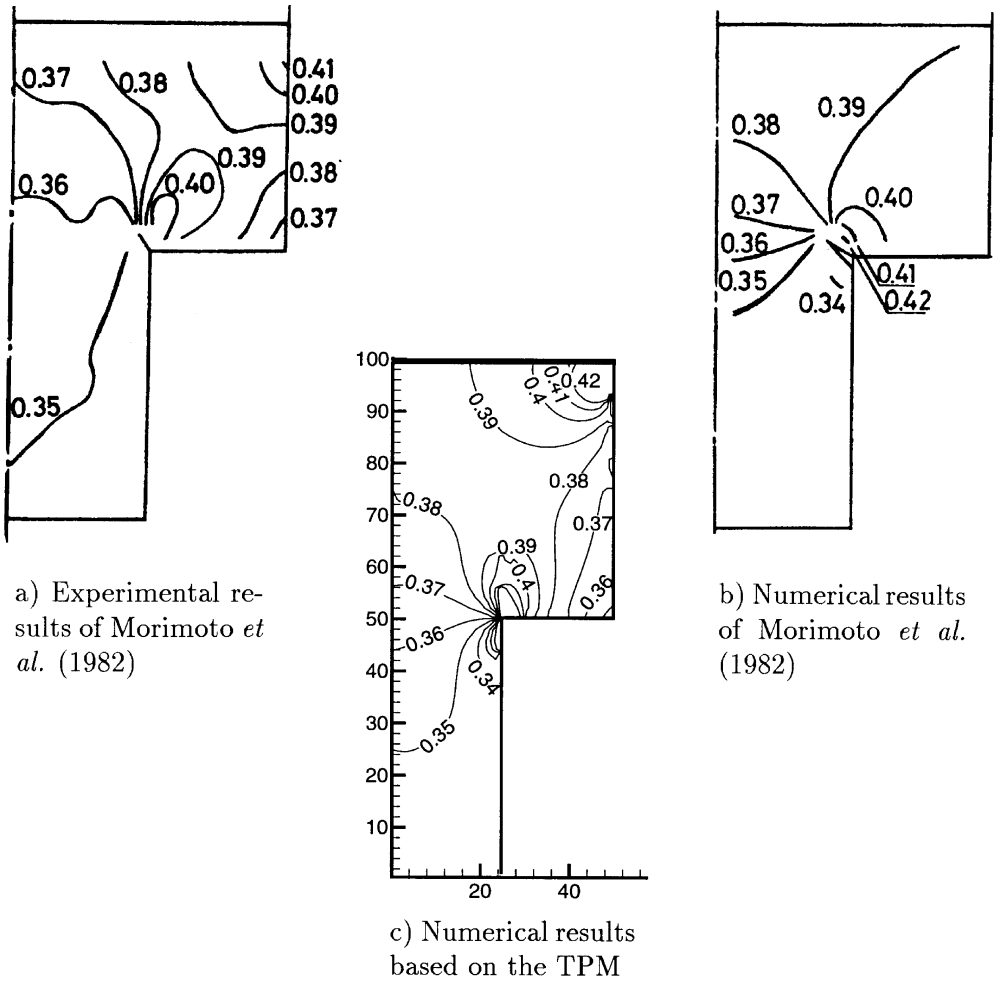

Fig. 10. Relative density (volume fraction of the solid) of the first case. (a) Experimental results of Morimoto et al. (1982). (b) Numerical results of Morimoto et al. (1982). (c) Numerical results based on the TPM.

is not explicitly given in the above mentioned article, only a remark, that the friction is small, caused by a die wall lubricant. Caused by this fact, the authors chose a friction factor of 0.02.

Figure 9 shows the relative density after 16 min, when the lower punch reaches its final displacement of 8 mm. The relative density at the lower part of the die increases much more than at the upper part. That is expected and analogous to the second investigation, see Fig. 10. Herein the upper punch moves down and the relative density at the upper part of the die increases more than the lower part.

The agreement between the numerical simulation based on the TPM and the experimental data is quite good. Only a small difference occurs at the lower right side. These areas of smaller relative density could have been caused by the friction factor assumed by the authors.

5.2. Die compaction—movement of the upper punch

In this investigation the bottom punch is fixed and the upper punch moves down with the same velocity as in Case 1. Coulomb's friction factor is 0.2 and the initial relative density is 0.332, as given in the above mentioned article.

Figure 9 exhibits the relative density of the metal powder after 16 min, when the upper punch reaches its final displacements of 8 mm. The numerical simulation of the die compaction based on the theory of porous media hits the experimental data much better than the numerical simulation of Morimoto et al. (1982). The compaction of the powder at the upper right side is totally left out in Morimoto et al.'s simulation, whereas the TPM approach represents this effect exactly. Also, the lower parts fits better to the experimental results.

The examples in Section 5 prove that the TPM is a powerful tool for the simulation of compaction of metal powders. In both the cases the numerical calculation with the TPM fits the experimental results.

6. Concluding remarks

In this investigation the elastic and the elastic-ideal-plastic material behavior of a fluid saturated porous medium has been taken into account. The governing equations are formulated by a model with two microscopic incompressible phases. Based on this model the classical one- and two-dimensional consolidation process, as well as the wave propagation in a two-dimensional plane has been calculated. The plastic material behavior is related to a compaction process of metal powder.

In the one-dimensional example the numerical results of the consolidation problem were compared with an existing analytical solution, based on the same theory. Only small differences occur between the numerical and analytical solutions. The presented two-dimensional example of a dynamic consolidation problem shows the expected behavior of the pore pressure distribution, the seepage velocity and the solid displacement. In the example of the two-dimensional wave propagation the well-known longitudinal wave as well as the shear wave can be observed.

The numerical simulations of the compaction processes are compared with experimental and numerical results and show a better agreement to the experimental data than the numerical approach done by Morimoto et al. (1982).

The presented theory is a convenient alternative to the well-known Biot's theory, as it presents a completely consistent procedure based on the fundamental balance equations of mechanics. For this reason, a further development, e.g., physical and geometrical non-linearities, as well as plastic material behavior can be implemented in a consistent way.

Acknowledgements

The authors are grateful to Prof. Dr-Ing. R. de Boer and Priv.-Doz. Dr-Ing. J. Bluhm for their critical comments offered during the preparation of this paper. This work has been supported by the Deutsche Forschungsgemeinschaft (Germany).

References

Bathe, K.J., 1990. Finite-Element-Methoden. Springer-Verlag, Berlin.
Biot, M.A., 1955. Theory of elasticity and consolidation for a porous anisotropic solid. J. Appl. Phys. 26, 182.
Biot, M.A., 1956. Theory of propagation of elastic waves in fluid-saturated porous soil. I. Low-frequency range. J. Acoust. Soc. Am. 28, 168.
Bluhm, J., 1997. A consistent model for empty and saturated porous media. Forschungsbericht aus dem Fachbereich Bauwesen, vol. 74. Essen.
Bluhm, J., de Boer, R., 1997. The volume fraction concept in the porous media theory. Zeitschr. Angew. Math. Mech. (ZAMM) 77 (8), 563.
Bluhm, J., de Boer, R., Skolnik, J., 1996. Allgemeine Plastizitätstheorie für poröse Medien. Forschungsbericht aus dem Fachbereich Bauwesen, vol. 73. Essen.
de Boer, R., 1982. Vektor- und Tensorrechnung für Ingenieure. Springer-Verlag, Berlin.
de Boer, R., 1996. Highlights in the historical development of the porous media theory: toward a consistent macroscopic theory. Appl. Mech. Rev. 49, 201.
de Boer R., Ehlers, W., 1980. Grundlagen der isothermen Plastizitäts- und Viskoplastizitätstheorie. Forschungsbericht aus dem Fachbereich Bauwesen, vol, 14. Essen.
de Boer, R., Kowalski, S., 1983. A plasticity theory of fluid-saturated porous solids. Int. J. Eng. Sci. 21, 1143–1357.
de Boer, R., Ehlers, W., Liu, Z., 1993. One-dimensional transient wave propagation in fluid-saturated incompressible porous media. Arch. of Appl. Mechanics 63, 59.
Bowen, R.M., 1980. Incompressible porous media models by use of the theory of mixtures. Int. J. Engng Sci. 18, 1129.
Breuer, S., 1997. Dynamic response of a fluid-saturated elastic porous solid. Arch. of Mech. 49 (4) 771.
Diebels, S., Ehlers, W., 1996. Dynamic analysis of a fully saturated porous medium accounting for geometrical and material non-linearities. Int. J. for Num. Meth. in Engng 39, 81–97.
Ehlers, W., 1989. Poröse Medien—ein kontinuumsmechanisches Modell auf der Basis der Mischungstheorie. Forschungsbericht aus dem Fachbereich Bauwesen, vol. 47. Essen.
Ehlers, W., Diebels, S., 1994. Dynamic deformations in the theory of fluid-saturated porous solid materials. Proc. of the IUTAM Symposium on Anisotropy, Inhomogeneity and Nonlinearity in Solid Mechanics. Nottingham, U.K.
Fillunger, P., 1936. Erdbaumechanik? Selbstverlag des Verfassers, Wien.
Green, R.J., 1972. A plasticity theory for porous solids. Int. J. Mech. Sci. 14, 215–224.
Lewis, R.W., Schrefler, B.A., 1987. The Finite Element Method in the Deformation and Consolidation of a Porous Media. John Wiley and Sons.
Morimoto, Y., Hayashi, T., Takei, T., 1982. Mechanical behavior of powders during compaction in a mold with variable cross sections. Int. J. Powder Metallurgy and Powder Technology 18, 2.
Morland, L.W., 1972. A simple constitutive theory for fluid-saturated porous solid. J. Geophys. Res. 88, 890–900.
Mow, V.C., Kuei, S.C., Lai, W.M., Armstrong, C.G., 1980. Biphasic creep and stress relaxation of articular cartilage in compression: theory and experiments. J. Biom. Engng 102, 73–84.
Nunziato, J.W., Passman, S.L., 1981. A multiphase mixture theory for fluid-saturated granular materials. In: Selvadurai, A.P.S. (Ed.), Mechanics of Structured Media. Elsevier, Amsterdam, pp. 243–254.
Prévost, J.H., 1981. Consolidation of anelastic porous media. J. Eng. Mech. Div., ASCE, 107 (EM1), 169–186.
Richart, F.E., Hall, J.R., Woods, R.D., 1970. Vibrations of Solids and Foundations. Prentice-Hall, New Jersey.
Stefan, J., 1871. Über das Gleichgewicht und die Bewegung, insbesondere die Diffiusion von Gasgemengen, Sitzungsber. Akad. Wiss., Math.-Naturwiss. K1, Abt. II a, Wien, pp. 63–124.
Truesdell, C., 1957. Sulle basi della termomeccanica. Rend. Linc. 22, 158.
Zienkiewicz, O.C., 1984. Methode der Finiten Elemente. Carl Hanser Verlag, München.
Zienkiewicz, O.C., Shiomi, T., 1984. Dynamical behaviour of saturated porous media; the generalized Biot formulation and its numerical solution. Int. J. Numer. Anal. Methods Geomechanics 8, 71.